# Electronic structure and Fermi surface of $CrO_2$

N. E. Brener and J. M. Tyler
*Department of Computer Science, Louisiana State University, Baton Rouge, Louisiana 70803-4020*

J. Callaway*
*Department of Physics and Astronomy, Louisiana State University, Baton Rouge, Louisiana 70803-4001*

D. Bagayoko and G. L. Zhao
*Department of Physics, Southern University, Baton Rouge, Louisiana 70813*
(Received 2 March 2000)

We report the results of an all electron self-consistent calculation of the electronic structure of $CrO_2$ in the local spin-density approximation, employing an extended version of the linear combination of Gaussian orbitals method. $CrO_2$ is found to be a half-metallic ferromagnet in agreement with previous calculations and recent experiments. The predicted Fermi surface is described in detail.

## I. INTRODUCTION

$CrO_2$ is unusual among $3d$ transition metal oxides in that it is both ferromagnetic and metallic in contrast to the more common occurrence of insulating antiferromagnets. It is believed to be a ''half-metallic ferromagnet,'' [1] one of a small class of materials in which an insulating gap separates occupied and unoccupied states of minority spin, while only electrons of majority spin participate in forming the Fermi surface.[2] Its magnetic and conducting properties make $CrO_2$ important in technology. In addition to being widely used as magnetic recording media, it has possible applications in spin-polarized electron tunneling devices since a half-metallic material can provide electrons that are 100% spin polarized. From a fundamental point of view, the well-known failures of the local spin-density approximation (LSDA) in density functional theory to predict the insulating, antiferromagnetic ground state of many transition-metal oxides make it interesting to see to what extent LSDA works for a similar but metallic system.

There have been several previous studies of this material. An early article by Goodenough[3] presented a phenomenological model for the electronic structure of metallic oxides. Band calculations in the LSDA have been reported by Schwartz,[1] Kulatov, and Mazin,[4] Sorantin and Schwartz,[5] Matar *et al.*,[6] Lewis, Allen, and Sazaki,[7] and Mazin, Singh, and Ambrosch-Draxl *et al.*[8] These papers emphasize bonding and magnetic properties; they agree that $CrO_2$ should be a half-metallic ferromagnet. An early experimental investigation of spin-resolved photoemission from $CrO_2$ films formed by chemical vapor decomposition[9] found that, although the emitted electrons were nearly 100% spin polarized for binding energies of 2.0 eV or less below the Fermi energy, a sharp Fermi edge could not be detected. This result is in sharp contradiction to the LSDA calculations reported and supports a localized picture of the magnetization, but is difficult to reconcile with the metallic character of $CrO_2$. However, in more recent photoemission measurements on bulk polycrystals of $CrO_2$, Tsujioka *et al.*[10] found a small but finite density of states at the Fermi level, consistent with its metallic behavior. In addition, Ranno, Barry, and Coey[11] measured magnetic and magnetotransport properties of $CrO_2$ films deposited on $Al_2O_3$ and $TiO_2$ and found that $CrO_2$ exhibits the behavior expected for a half-metallic ferromagnet. Thus recent experiments support the LSDA prediction of the half-metallic character of $CrO_2$. Additional experiments would be desirable to further clarify this matter and provide more information regarding the possible use of $CrO_2$ as a source of spin-polarized electrons.

We think it would be useful to make specific predictions of the Fermi surface in $CrO_2$ as a possible stimulus to further experimental investigations. To this end, we report the results of self-consistent all electron LSDA calculations of the band structure, density of states, and Fermi surface. The calculation is made using the full potential LCGO (linear combination of Gaussian orbitals) method.[12] This procedure, which has been documented in the literature,[12,13] has been modified to accommodate the tetragonal symmetry of this material. Our improved method is described in Sec. II. The band structure and density of states, which are in rather good agreement with published results, are shown in Sec. III. The Fermi surface, surprisingly complex, is also described in this section. The recent paper by Mazin, Singh, and Ambrosch-Draxl[8] also shows the $CrO_2$ Fermi surface. While the Fermi surface given in the Mazin, Singh, and Ambrosch-Draxl paper has a similar shape to the one reported here, there are several important differences. These differences are discussed in Sec. III.

## II. METHOD OF CALCULATION

The $CrO_2$ calculations described in this paper were done with a new, general version of the program BANDPACKAGE. The original version of BANDPACKAGE, which is restricted to cubic symmetry and one atom per unit cell, is described in Refs. 12 and 13 and has been used to perform energy-band calculations on a number of cubic metals. The new, general version of BANDPACKAGE can be applied to crystals with an arbitrary number of atoms per unit cell and can be adapted to a number of different crystal symmetries. Both the original

 

and general versions of BANDPACKAGE have several advantages compared to other methods in current use, including the following:

(1) BANDPACKAGE makes no shape (e.g., muffin-tin) approximations concerning the crystal potential.

(2) BANDPACKAGE yields analytic, rather than numerical, wave functions. The use of analytic wave functions makes it much easier to compute the matrix elements involved in quantities such as Compton profiles, optical conductivities, dielectric functions, and susceptibilities, since the needed integrals can be done analytically rather than numerically. This is particularly true when the matrix elements involve derivatives, as in the case of the optical conductivity.

We now give a brief outline of the computational method used in the general version of BANDPACKAGE. This method is a generalization of the procedure given in Refs. 12 and 13. The general version of BANDPACKAGE employs the LCGO method in which the one-electron wave function $\Psi_l$ is expanded in Gaussian orbitals:

$$\Psi_l(\mathbf{k},\mathbf{r}) = \sum_{mi} C_{lmi}(\mathbf{k})\varphi_{mi}(\mathbf{k},\mathbf{r}) \tag{1}$$

$$\varphi_{mi}(\mathbf{k},\mathbf{r}) = \frac{1}{\sqrt{N}} \sum_{\mu} e^{i\mathbf{k}\cdot(\mathbf{R}_\mu+\mathbf{r})} u_{mi}(\mathbf{r}-\mathbf{R}_\mu-\mathbf{r}_m) \tag{2}$$

where the $C_{lmi}$ are expansion coefficients, the $\varphi_{mi}$ are Bloch functions, the $u_{mi}$ are atomic orbitals (Gaussians), the index $m$ goes over atoms in the unit cell, the index $i$ goes over atomic orbitals on atom $m$, $\mathbf{k}$ is a reciprocal space vector, $\mathbf{R}_\mu$ is a direct lattice vector, $\mathbf{r}_m$ is the vector from the origin of the unit cell to atom $m$, $l$ is a band index, and $N$ is the number of unit cells in the crystal. The phase factor $e^{i\mathbf{k}\cdot\mathbf{r}_m}$ has been inserted in Eq. (2) for reasons of computational convenience.

The crystal potential $V$ is written as a Coulomb potential $V_C$ and a local density exchange-correlation potential $V_{xc}$:

$$V(\mathbf{r}) = V_C(\mathbf{r}) + V_{xc}(\mathbf{r}) \tag{3}$$

where the exchange-correlation potential used in the present calculations is the von Barth-Hedin form as parameterized by Rajagopal, Singhal, and Kimball.[14] We write the Coulomb potential as a nuclear part plus an electronic part:

$$V_C(\mathbf{r}) = V_C^{\text{nuc}}(\mathbf{r}) + V_C^{\text{elec}}(\mathbf{r}) \tag{4}$$

$$V_C^{\text{nuc}}(\mathbf{r}) = -\sum_{\mu m} \frac{Z_m e^2}{|\mathbf{r}-\mathbf{R}_\mu-\mathbf{r}_m|} \tag{5}$$

$$V_C^{\text{elec}}(\mathbf{r}) = e^2 \int \frac{\rho(\mathbf{r}')}{|\mathbf{r}-\mathbf{r}'|} d^3r' \tag{6}$$

where $Z_m$ is the atomic number of atom $m$, $e$ is the charge of an electron, and $\rho$ is the electronic charge density. In the first iteration of the self-consistent calculation, we set the electronic charge density equal to the sum of the atomic charge densities:

$$\rho(\mathbf{r}) = \sum_{\mu m} \rho_m(\mathbf{r}-\mathbf{R}_\mu-\mathbf{r}_m) \tag{7}$$

where $\rho_m$ is the electronic charge density of atom $m$.

In order to facilitate the computation of the Hamiltonian matrix elements, we expand the crystal potential in a Fourier series in reciprocal lattice vectors $\mathbf{K}$:

$$V(\mathbf{r}) = \sum_{\mathbf{K}} V(\mathbf{K}) e^{i\mathbf{K}\cdot\mathbf{r}}. \tag{8}$$

The Fourier coefficients of the nuclear part of the Coulomb potential are given by

$$V_C^{\text{nuc}}(\mathbf{K}) = -\frac{8\pi}{\Omega K^2} \sum_m Z_m e^{-i\mathbf{K}\cdot\mathbf{r}_m} \tag{9}$$

where $\Omega$ is the volume of the unit cell in the direct lattice and we have used atomic units in which $e^2=2$. In the first iteration, the Fourier coefficients of the electronic part of the Coulomb potential are given by

$$V_C^{\text{elec}}(\mathbf{K}) = \frac{8\pi}{K^2}\rho(\mathbf{K}) \tag{10}$$

$$\rho(\mathbf{K}) = \frac{1}{\Omega}\sum_m e^{-i\mathbf{K}\cdot\mathbf{r}_m} \int \rho_m(\mathbf{r}) e^{-i\mathbf{K}\cdot\mathbf{r}} d^3r \tag{11}$$

where the origin for the integral in Eq. (11) is atom $m$ and the integral is over all space.

The Fourier coefficients of the exchange-correlation potential $V_{xc}(\mathbf{K})$ are calculated as follows:

$$V_{xc}(\mathbf{K}) = V_{xc}^{\text{sphs}}(\mathbf{K}) + V_{xc}^{\text{int}}(\mathbf{K}) \tag{12}$$

where $V_{xc}^{\text{sphs}}(\mathbf{K})$ and $V_{xc}^{\text{int}}(\mathbf{K})$ are the contributions of atomic spheres centered on the atoms and of the interstitial region, respectively. This procedure has been described in Ref. 15 for a crystal with one atom per unit cell. For the case of more than one atom per unit cell, $V_{xc}^{\text{sphs}}(\mathbf{K})$ and $V_{xc}^{\text{int}}(\mathbf{K})$ are given by

$$V_{xc}^{\text{sphs}}(\mathbf{K}) = \frac{1}{\Omega}\sum_m e^{-i\mathbf{K}\cdot\mathbf{r}_m} \int_{\text{sphs}} V_{xc}(\mathbf{r}) e^{-i\mathbf{K}\cdot(\mathbf{r}-\mathbf{r}_m)} d^3r \tag{13}$$

$$V_{xc}^{\text{int}}(\mathbf{K}) = \overline{V}_{xc}^{\text{int}}(\mathbf{K}) - \frac{1}{\Omega}\sum_{\mathbf{K}'} \overline{V}_{xc}^{\text{int}}(\mathbf{K}') \sum_m e^{-i(\mathbf{K}-\mathbf{K}')\mathbf{r}_m} \begin{cases} \frac{4}{3}\pi a_m^3 & \mathbf{K}'=\mathbf{K} \\ \frac{4\pi a_m^2}{|\mathbf{K}-\mathbf{K}'|} j_1(|\mathbf{K}-\mathbf{K}'|a_m) & \mathbf{K}'\neq\mathbf{K} \end{cases} \tag{14}$$

where the integrals in Eq. (13) are over atomic spheres centered on the atoms, $a_m$ is the radius of sphere $m$, $j_1$ is a spherical Bessel function of $l=1$, $\mathbf{K}'$ is a reciprocal lattice vector, and the Fourier coefficients $\mathbf{V}_{xc}^{\text{int}}(\mathbf{K}')$ are obtained by a least-squares fit to the exchange-correlation potential in the interstitial region. The atomic spheres are chosen to be small enough so that the exchange-correlation potential inside the spheres can be treated as being spherically symmetric, in which case the integrals over the spheres can easily be done numerically. The least-squares fit in the interstitial region can be done to a high degree of accuracy by using a sufficient number of reciprocal lattice vectors in the fit.

As shown in Eq. (1), the Bloch functions $\varphi_{mi}$ are the basis functions in the LCGO method. The matrix elements of the potential with respect to the Bloch functions are given by

$$V_{mi,nj}(\mathbf{k})=\sum_{\mu} e^{-i\mathbf{k}\cdot(\mathbf{R}_\mu+\mathbf{r}_m-\mathbf{r}_n)}\sum_{\mathbf{K}} V(\mathbf{K}) \times \int u_{mi}^{*}(\mathbf{r}-\mathbf{R}_\mu-\mathbf{r}_m+\mathbf{r}_n)e^{i\mathbf{K}\cdot(\mathbf{r}+\mathbf{r}_n)}u_{nj}(\mathbf{r})d^3r. \tag{15}$$

The evaluation of the integrals in Eq. (15) has been described in Ref. 12 for the case of cubic symmetry. For crystals with arbitrary symmetry, the evaluation of these integrals is a straightforward generalization of the procedure given in Ref. 12. Convergence of the reciprocal lattice sums is speeded up by employing a model potential that is added to the Fourier series expansion for $V(r)$ and subtracted by computing its matrix elements in direct space.[12]

In the self-consistency procedure, the new charge density obtained in each iteration is given by

$$\rho(\mathbf{r})=\sum_{\mathbf{k},l\ \text{occ.}} |\Psi_l(\mathbf{k},\mathbf{r})|^2 \tag{16}$$

where the sum on $\mathbf{k}$ is over the first Brillouin zone and the sum on $l$ is over occupied states only. Using Eq. (16), we obtain the following expression for the Fourier coefficients of the charge density:

$$\rho(\mathbf{K})=\frac{1}{N\Omega}\sum_{\mathbf{k},l\ \text{occ.}}\sum_{\min j} c_{lmi}^{*}(\mathbf{k})c_{lnj}(\mathbf{k})S_{mi,nj}(\mathbf{k},\mathbf{K}) \tag{17}$$

$$S_{mi,nj}(\mathbf{k},\mathbf{K})=\sum_{\mu} e^{-i\mathbf{k}\cdot(\mathbf{R}_\mu+\mathbf{r}_m-\mathbf{r}_n)} \times \int u_{mi}^{*}(\mathbf{r}-\mathbf{R}_\mu-\mathbf{r}_m+\mathbf{r}_n) \times e^{-i\mathbf{K}\cdot(\mathbf{r}+\mathbf{r}_n)}u_{nj}(\mathbf{r})d^3r. \tag{18}$$

The self-consistent, spin-polarized $CrO_2$ calculations reported in this paper were done using the generalized LCGO method outlined above. In these calculations, 600 independent reciprocal lattice vectors were used to fit the exchange-correlation potential in the interstitial region. During the self-consistency process, only the first 40 Fourier coefficients of the potential were allowed to change, since the changes become very small by the 40th coefficient. The self-consistent iterations were continued until the potential coefficients converged to $10^{-5}$. The atomic orbital (Gaussian) basis set used in these calculations is obtained primarily from the basis sets

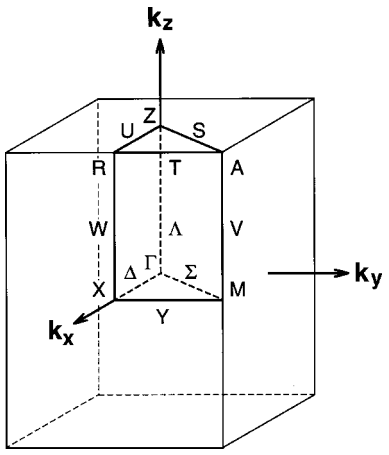


FIG. 1. Brillouin Zone for $CrO_2$ (tetragonal lattice). The points and lines of symmetry that define the irreducible wedge are shown according to Ref. 18.

for Cr and O given by Wachters[16] and Poirier, Kari, and Csizmadia,[17] respectively. This basis set has $13s$, $9p$, and $3d$ orbitals for each of the two Cr atoms in the unit cell, and $6s$ and $4p$ orbitals for each of the four O atoms. The exponents and coefficients used in this basis set are available on request. There are a total of 182 atomic basis functions. Thus in order to obtain the $CrO_2$ energy bands, we diagonalized a $182\times182$ complex Hamiltonian matrix at each $k$ point used in the calculations. 24 $\mathbf{k}$ points in the irreducible section of the Brillouin zone were used in the self-consistent iterations, and the self-consistent potential so obtained was then employed to calculate the energy bands at 585 $\mathbf{k}$ points in the irreducible section of the zone. The $CrO_2$ lattice constants[1] used in the present calculations are $a=4.421A$, $c=2.916A$, and $u=0.3053$.

## III. RESULTS

### A. Band structure and density of states

The Brillouin zone for the tetragonal structure is shown in Fig. 1, which also illustrates the points and lines of symmetry in the irreducible wedge, according to Mattheiss.[18]

The overall magnetic moment is $2.0\mu_B$ per Cr atom, in agreement with experiment.[19]

The bands near the Fermi energy are shown in Fig. 2 for

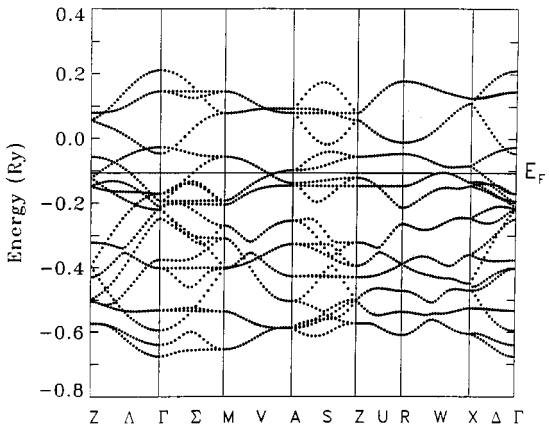


FIG. 2. Majority spin bands.

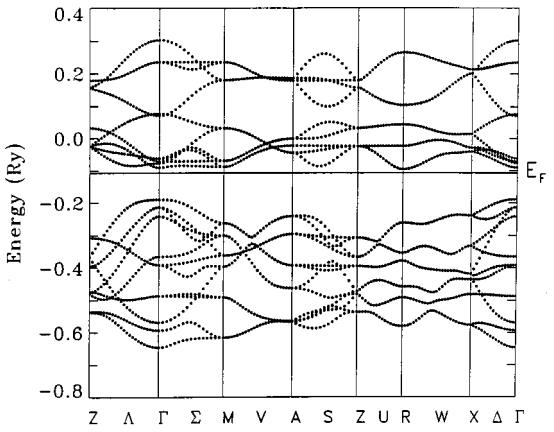


FIG. 3. Minority spin bands.

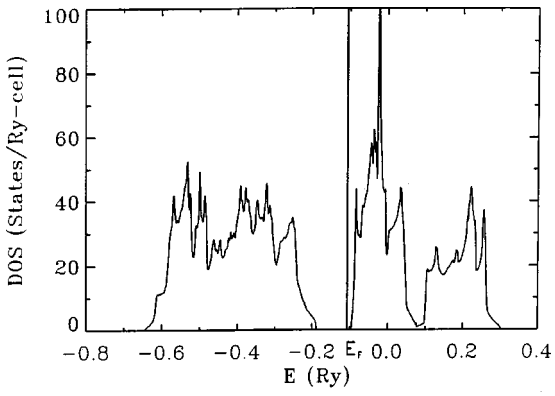


FIG. 5. Minority spin density of states.

majority spin (↑) and in Fig. 3 for minority spin (↓). Our results appear to be in good agreement with other calculations.[1,5,6] The bands shown are formed by the hybridization of O $(2p)$ and Cr $(3d)$ orbitals. The bottom of this complex is about 9.5 eV above the O $(2s)$ bands, which are not shown in the figures. The densities of states are shown in Figs. 4 and 5.

The figures illustrate the half metallic nature of $CrO_2$. The minority spin bands are separated by a minimum gap of 1.34 eV (at $\mathbf{k}=0$). The Fermi energy is in this gap, so that at $T=0$, the ↓ states below the gap are full, and those above it are empty. The Fermi energy does intersect the majority spin bands: the ↑ electrons are metallic, and the Fermi surface will be described below. The density of states at the Fermi energy is 31.671/(cell Ry).

Although an ionic picture of the electronic structure cannot be accepted without some reservations, it does suggest a qualitative explanation of the major features. In this view, the O $(2p)$ bands are full. This is easy to see from the ↓ band structure of Fig. 3 in which bands holding 12 electrons per cell lie below the Fermi energy. We might suppose that four electrons per atom (of both spins) have transferred from Cr to O, leaving $Cr^{4+}$ ions in a $d^2$ configuration. These spins align in accord with Hund's rule. (The ground state of a $Cr^{4+}$ ion is $^3F$). It is also clear from the figures that the upper bands, which are predominately Cr $(3d)$, are split into a lower set that can hold 6 electrons per cell $(t_{2g})$ and an upper set that can hold 4 $(e_g)$. The $t_{2g}$ and $e_g$ groups of bands overlap only slightly. There are 2 Cr $(3d)$ electrons per atom, already spin polarized, to occupy a band complex that can hold 3. Hence the system is metallic, and the Fermi level in Fig. 2 is in the upper part of the $t_{2g}$ group of bands. Moreover, since the electrons are already spin polarized, we do not expect additional strong correlations that would further split the $t_{2g}$ complex to yield an insulator. Even though the Fermi energy falls in a minimum of the ↑ density of states, we think it is probable that the $d$ ↑ electrons remain metallic, as our calculation predicts. There is some controversy in regard to this point, which will be discussed subsequently.

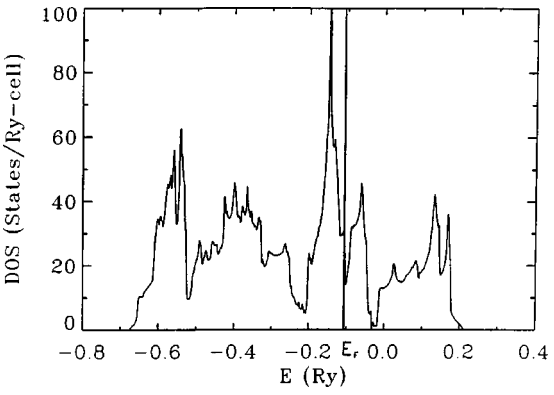


FIG. 4. Majority spin density of states.

Although the ionic picture explains both the magnetic moment and the metallic behavior, it fails in regard to the distribution of charge. The calculations of Schwarz[1] and Matar *et al.*[6] find about four electrons (above the core) inside the Wigner Seitz spheres around the chromium atoms. However, the excess charge (with respect to the ionic picture) is associated with $p$-$d$ hybridization—the charge belongs to wave functions that are $p$-like on oxygen but retain $d$ symmetry about Cr. Since both ↑ and ↓ states of these hybridized bands are occupied, this $d$ charge is magnetically inert, leaving the two remaining $d$ electrons on each site free to couple their spins ferromagnetically, in accord with Hund's rule.

The calculated $d$ spin splittings support this ionic plus covalent picture. The exchange splitting of the predominately O $(2p)$ bands is not zero, as it presumably would be in a purely ionic picture, but it is small. At the top of the O $(2p)$ complex, comparison of the energies of corresponding states reveals a quite small splitting of about 0.1 eV. It is larger at the bottom, about 0.4 eV, where we have bonding $pd\sigma$ orbitals, but the spin splitting in the predominately Cr $(3d)$ bands is much larger, mostly in the range of 1.3–1.6 eV. From the band view point, it is the difference in exchange splittings of the $p$ and $d$ states that is responsible for the half-metallic properties: the ↑ $d$ states are lowered and the ↓ $d$ states are raised with respect to the weakly split $p$ states to the extent that the $d$ ↑ states overlap the $p$ in energy and the $d$ ↓ are raised above the Fermi energy.

### B. The Fermi surface

It is seen in Fig. 2 that the Fermi energy intersects the ↑ band in several places. This leads to a complex Fermi surface that has both large hole and large electron portions. $CrO_2$ is a compensated metal.

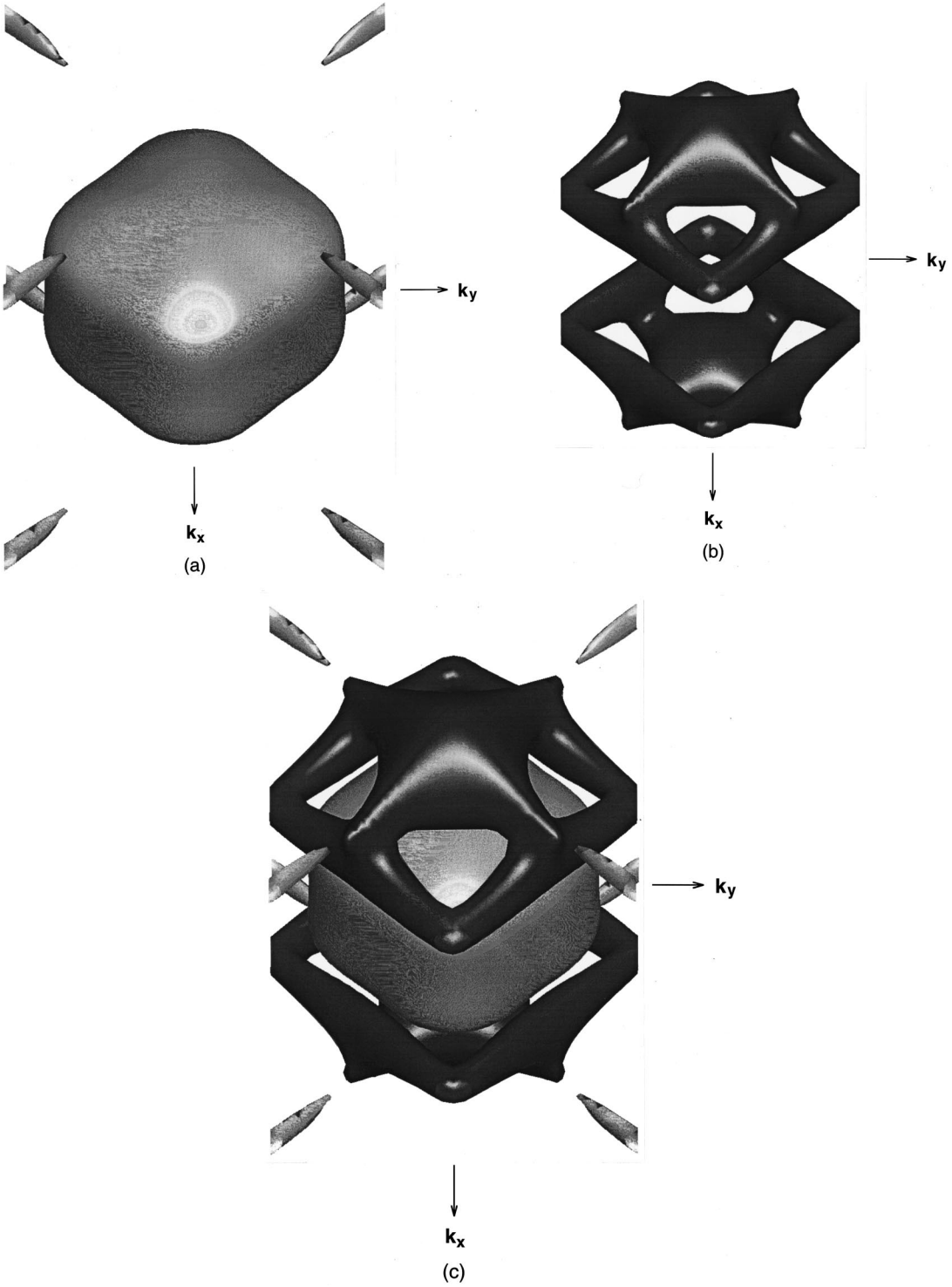


FIG. 6. (a) Electron Fermi surface: pillbox and needles. (b) Hole Fermi surface: the Crabs. (c) Electron Fermi surface (light) and hole Fermi surface (dark).

There is a large, closed, electron surface, ''the pill box,'' around the zone center, extending about 40% of the $\Gamma$-$Z$ distance on the $k_z$ axis. It is shown in Fig. 6(a) in a three-dimensional picture. The surface is relatively flat on top. There are also two cross-shaped surfaces (one above the pill box and one below) centered on the zone edges, each with four thin, needle shaped arms that run into the zone from the edges parallel to the $\Sigma$ axes. As shown in Fig. 6(a), these eight arms are separate structures inside the first Brillouin zone but will form closed, cross-shaped surfaces if four zones are placed together at an edge. Cross sections of these portions of the Fermi surface in the $\Gamma MAZ$ plane are shown in Fig. 7, and in the $\Gamma XRZ$ plane in Fig. 8.

There is also a large hole Fermi surface, shown in a three-dimensional view in Fig. 6(b) (''the Crabs''). Cross sections are shown in the $\Gamma MAZ$ plane (Fig. 7) and the $\Gamma XRZ$ plane (Fig. 8). This surface does not extend to the top of the Brillouin zone, nor does it include the center. There are two

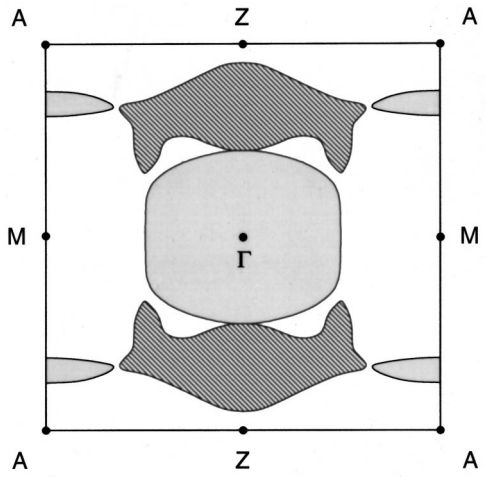


FIG. 7. Cross section of the electron Fermi surface (shaded) and hole Fermi surface (lined) in the ΓMAZ plane.

crabs; the long thin arms run around the body of the zone. The hole and electron surfaces are shown together in Fig. 6(c).

Figure 9 shows cross sections of the Fermi surface in the faces of the irreducible wedge of the Brillouin zone. The top face (ZRA) is not shown in the figure because there is no Fermi surface in this face.

The $CrO_2$ Fermi surface reported by Mazin, Singh, and Ambrosch-Draxl[8] has a similar shape to the one given here, however, there are several important differences:

(1) The hole surface in the Mazin paper has hammerheads that are separated from each other by gaps. As a result of the gaps between the hammerheads, this hole surface does not make contact with the sides of the Brillouin zone. In contrast, the hole surface given here does not have hammerheads but instead has a continuous band that touches the sides of the zone at circles centered on the *W* axes.

(2) The hole surface in the Mazin paper touches the top of the Brillouin zone at the *Z* point, whereas the hole surface given here does not make contact with the top of the zone.

(3) The electron surface given here includes eight needle-shaped arms that are aligned parallel to the *S* axes. Such

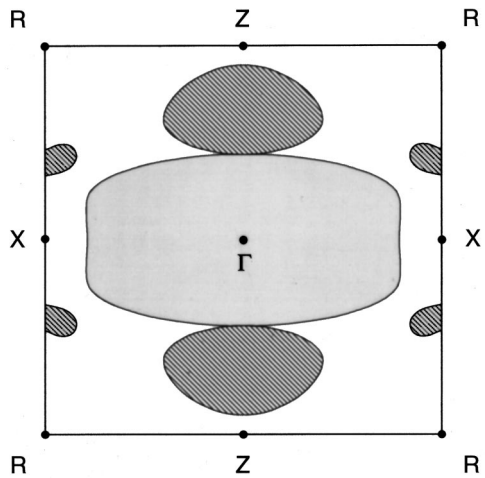


FIG. 8. Cross section of the electron Fermi surface (shaded) and hole Fermi surface (lined) in the ΓXRZ $(k_y=0)$ plane.

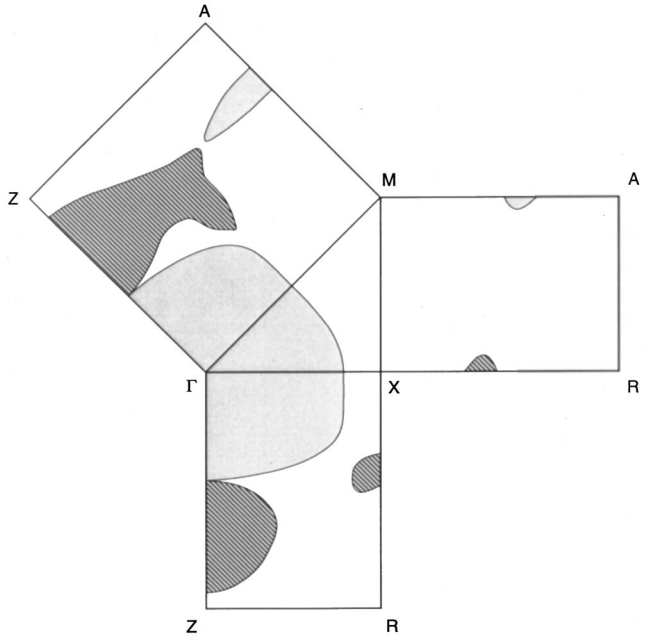


FIG. 9. Cross sections of the electron Fermi surface (shaded) and hole Fermi surface (lined) in the faces of the irreducible wedge.

electron structures are mentioned in the Mazin paper but are not shown.

Table I gives cross sectional areas of the Fermi surface in the ΓXM $(k_z=0)$, ΓMAZ, and ΓXRZ planes. For each plane, the table lists the areas of only the largest surfaces, all of which are closed surfaces in the full Brillouin zone. The largest cross section for the electron surfaces is in the ΓXRZ plane, while the largest one for the hole surfaces is in the ΓMAZ plane. The areas given in Table I are extremal cross sections of the Fermi surface. They can be measured experimentally, since the frequency of high-field and low-temperature de Haas-van Alphen oscillations of the magnetic susceptibility is proportional to the area of extremal cross sections of the Fermi surface normal to the direction of the field.

Table II gives values of the effective mass $m^*$ for orbits around the extremal cross-sectional areas of the Fermi surface. The effective mass is proportional to the derivative of the cross-sectional area with respect to energy, evaluated at the Fermi energy, according to the equation

$$m^* = \frac{1}{2\pi}\frac{\partial A}{\partial E}. \tag{19}$$

We approximated these derivatives with ratios of changes in the areas $\Delta A$ to corresponding changes in the energy $\Delta E$.

TABLE I. Extremal cross-sectional areas of the Fermi surface of $CrO_2$, in units of area in reciprocal space.

| | ΓXM | ΓMAZ | ΓXRZ |
|---|---|---|---|
| Electron surfaces | 0.25 | 0.23 | 0.26 |
| Hole surfaces | | 0.12 | 0.06 |

TABLE II. Effective masses for selected orbits, in units of free electron mass.

| | ΓXM | ΓMAZ | ΓXRZ | *X*MAR |
|---|---|---|---|---|
| Electron orbits | 0.48 | 0.49 | 0.58 | |
| Hole orbit | | | | −0.50 |

We used values for $\Delta E$ of 0.01 and 0.005 Ry around the Fermi energy and averaged the results from these two values to obtain the effective masses listed in Table II. For a given plane, only the largest cross-sectional area has been considered in these calculations. As shown in the table, the largest electron effective mass is the one for an orbit in the ΓXRZ plane. We note that the hole effective mass is negative, in agreement with Hall-effect measurements. These values of the effective mass should permit additional comparisons with experiment, as $m^*$ appears in several measured quantities including the cyclotron frequency and the transverse Hall voltage.

## IV. SUMMARY AND CONCLUDING REMARKS

In summary, we have made a full potential, all electron, self-consistent calculation of the electronic structure of $CrO_2$ using the LSDA and an improved form of the LCGO method. The LCGO method, as revised, was briefly described. We found that $CrO_2$ is a half-metallic ferromagnet, in agreement with previous calculations[1,4–8] and recent experiments,[10,11] and in sharp contrast to an earlier photoemission experiment that failed to find a Fermi edge.[9] The principal contribution of this work is a detailed description of the predicted Fermi surface. We think that additional measurements relevant to the Fermi surface are particularly important because of the clear contrast between the earlier photoemission experiment and both theoretical and recent experimental work. Such measurements could also provide additional information regarding the possible use of $CrO_2$ in devices that require spin-polarized electrons.

Our predictions concerning the Fermi surface should be testable either through photoemission or de Haas-van Alphen effect measurements provided that single crystals can be grown. We think such measurements would be of great interest regarding the ability of density functional theory to describe an unusual, metallic, transition-metal oxide.

## ACKNOWLEDGMENTS

This research was supported by the National Science Foundation under Grant Nos. HRD 91-08590 and DMR 91-20166, by the Louisiana Board of Regents under Contract No. NSF/LaSER (1993)-HRD-05, and by IBM Corporation.

*Deceased.

[1] K. Schwarz, J. Phys. F: Met. Phys. **16**, L211 (1986).

[2] R. A. de Groot, F. M. Mueller, P. G. van Ergen, and K. H. J. Buschow, Phys. Rev. Lett. **50**, 2024 (1983).

[3] J. G. Goodenough, in *Progress in Solid State Chemistry*, edited by H. Reiss (Pergamon, Oxford, 1971), Vol. 5, p. 145.

[4] E. Kulatov and I. I. Mazin, J. Phys.: Condens. Matter **2**, 343 (1990).

[5] P. I. Sorantin and K. Schwarz, Inorg. Chem. **31**, 567 (1992).

[6] S. Matar, G. Demazeau, J. Sticht, V. Egert, and J. Kubler, J. Phys. I **2**, 315 (1992).

[7] S. P. Lewis, P. B. Allen, and T. Sazaki, Phys. Rev. B **55**, 10 253 (1997).

[8] I. I. Mazin, D. J. Singh, and C. Ambrosch-Draxl, Phys. Rev. B **59**, 411 (1999).

[9] K. P. Kamper, W. Schmitt, G. Guntherodt, R. J. Gambino, and R. Ruf, Phys. Rev. Lett. **59**, 2788 (1987).

[10] T. Tsujioka, T. Mizokawa, J. Okamoto, A. Fujimori, M. Nohara, H. Takagi, K. Yamaura, and M. Takano, Phys. Rev. B **56**, R15 509 (1997).

[11] L. Ranno, A. Barry, and J. M. D. Coey, J. Appl. Phys. **81**, 5774 (1997).

[12] C. S. Wang and J. Callaway, Comput. Phys. Commun. **14**, 327 (1978).

[13] N. E. Brener, J. Callaway, and J. M. Tyler, in *Modern Techniques in Computational Chemistry—MOTECC-90*, edited by E. Clementi (Leiden, Escom, 1990), p. 785.

[14] A. K. Rajagopal, S. P. Singhal, and J. Kimball (unpublished), as quoted by A. K. Rajagopal in *Advances in Chemical Physics*, edited by G. I. Prigogine and S. A. Rice (Wiley, New York, 1979), Vol. 41, p. 59.

[15] P. Blaha and J. Callaway, Phys. Rev. B **32**, 7664 (1985).

[16] A. J. H. Wachters, J. Chem. Phys. **52**, 1033 (1970).

[17] R. Poirier, R. Kari, and I. Csizmadia, Physical Sciences Data 34: Handbook of Gaussian Basis Sets (Elsevier, Amsterdam, 1985), p. 9485.

[18] L. F. Mattheiss, Phys. Rev. B **13**, 2433 (1976).

[19] B. Kubota, J. Phys. Soc. Jpn. **15**, 1706 (1960).